Corner Detection Using the Affine Morphological Scale Space

Luis Alvarez(✉)

Departamento de Informática y Sistemas,
Universidad de Las Palmas de Gran Canaria,
Campus de Tafira, 35017 Las Palmas de Gran Canaria, Spain
lalvarez@ulpgc.es

Abstract. We introduce a method for corner estimation based on the affine morphological scale space (AMSS). Using some explicit known formula about corner evolution across AMSS, proven by Alvarez and Morales in 1997, we define a morphological cornerness measure based on the expected evolution of an ideal corner across AMSS. We define a new procedure to track the corner motion across AMSS. To evaluate the accuracy of the method we study in details the results for a collection of synthetic corners with angles from 15 to 160°. We also present experiments in real images and we show that the proposed method can also automatically handle the case of multiple junctions.

Keywords: Affine scale space · Corner detection · Morphology

1 Introduction

Corners are very important image features used in a lot of Computer Vision tasks. In this paper we present a morphological approach based on the theoretical results introduced in [5] about the evolution of an ideal corner in the affine invariant scale space (AMSS). This scale space, which was introduced in [4], is generated by the partial differential equation

$$\frac{\partial u}{\partial t} = (\mathcal{L}(u))^{\frac{1}{3}} \tag{1}$$

where

$$\mathcal{L}(u) = \left(\frac{\partial u}{\partial x}\right)^2 \frac{\partial^2 u}{\partial y^2} - 2\frac{\partial u}{\partial x}\frac{\partial u}{\partial y}\frac{\partial^2 u}{\partial x \partial y} + \left(\frac{\partial u}{\partial y}\right)^2 \frac{\partial^2 u}{\partial x^2} \tag{2}$$

A corner is defined by a corner tip $\bar{x}_0$, an angle α and a corner bisector unit vector $\hat{u}$. In [5], authors show that under the action of AMSS, a corner tip moves in the corner bisector direction in the following way:

$$\bar{x}(t) = \bar{x}_0 + \lambda \left(\frac{4}{3}t\right)^{\frac{3}{4}} \hat{u}, \tag{3}$$

F. Lauze et al. (Eds.): SSVM 2017, LNCS 10302, pp. 29–40, 2017.
DOI: 10.1007/978-3-319-58771-4_3

where

$$tan(\frac{\alpha}{2}) = \frac{1}{\lambda^2}. \tag{4}$$

The existence of a simple closed-form solution for the evolution of corners is something unique to AMSS. The evolution of corners in the linear scale spaces, or other morphological scale space as the one generated by the mean curvature motion, is much more complex and, as far as we know, there is not exist a closed-form solution in such cases. In this paper we exploit this nice behavior of AMSS to develop a robust and accurate technique to estimate corners in images. From Eq. (3) we obtain, on the one hand, that the evolution of the corner tip $\bar{x}(t)$ lies in the corner bisector and the orientation, $\hat{u}$, of the corner bisector is parallel to the image gradient in the corner tip $\bar{x}(t)$ (that is the curve normal direction), and on the other hand, for any interval $[t_0, t^*]$, the evolution of $\|\bar{x}(t) - \bar{x}(t_0)\|$ is linear with respect to $t^{\frac{3}{4}}$ for $t \in [t_0, t^*]$. Therefore we can perform a linear approximation of $\|\bar{x}(t) - \bar{x}(t_0)\|$ and the quality of such linear approximation can be used as a cornerness measure. Moreover, using Eq. (4) the slope of such linear approximation can be used to estimate the corner angle.

This paper is an extension of the work presented in [5]. The main contribution of this paper is a new method to define and track the corner evolution across AMSS using the local extrema of the operator $\mathcal{L}(u)$ defined in (2). Using this tracking procedure we define a cornerness measure based on the theoretical results introduced in [5]. We also present a detailed analysis of the associated corner detection algorithm, we study experimentally, the influence of the corner angle in the accuracy of the corner estimation and we study the application of the method to the detection of corner and multiple junctions in real images.

The rest of the paper is organized in the following way: in Sect. 2, we present some related works. In Sect. 3, we present in details the proposed corner detection algorithm. In Sect. 4, we present some experiments on synthetic and real images. In particular we use a collection of synthetic corner angles that we use to check the accuracy of the method for a range of angles. Finally, in Sect. 5, we present some conclusions.

2 Related Work

AMSS in terms of curve evolution have been introduced in [12,13]. The existence theory of a classic affine curve evolution was completed in [6]. The level set formulation in the sense of Osher and Sethian [11] for AMSS was developed in [2–4]. More recently, in [1], the authors present an application of AMSS to the computation of affine invariant distances.

The estimation of image features in the image is a common basic step in a lot of computer vision tasks. The well-known Harris technique, [8], is the reference technique for corner estimation, it introduces a cornernes measure based on the structure tensor. More recently, a lot of attention has been devoted to the SIFT method introduced in [9] to extract image features. In [14], a generalization to the affine invariant case of SIFT method is proposed. In [7], a study about

morphologically invariant descriptors is presented. In [10], a technique for corner estimation using the mean curvature scale space is proposed.

In [5], authors define an ideal corner of angle α as the following set:

$$X_\lambda = \{\bar{x} = (x, y) : y \geq \lambda^2 |x|\} \tag{5}$$

where λ is given by (4). Since Eq. (1) is morphologically invariant, the evolution of the corner X_λ is determined by any solution $u_\lambda(t, \bar{x})$ of (1) which includes X_λ as a level set of $u_\lambda(0, \bar{x})$. In particular, in [5], it is shown that for any increasing function $\phi(.)$ the following function is a solution of (1)

$$u_\lambda(t, \bar{x}) = \begin{cases} \phi\left(\left(\frac{y^2}{\lambda^2} - \lambda^2 x^2\right)^{\frac{2}{3}} - \frac{4}{3}t\right) & \text{if } \frac{y^2}{\lambda^2} - \lambda^2 x^2 \geq \left(\frac{4}{3}t\right)^{\frac{3}{2}} \\ 0 & \text{if } \frac{y^2}{\lambda^2} - \lambda^2 x^2 < \left(\frac{4}{3}t\right)^{\frac{3}{2}} \end{cases} \tag{6}$$

and then, the evolution of the corner X_λ is given by

$$X_\lambda = \left\{\bar{x} = (x, y) : y \geq \lambda\left(\lambda^2 x^2 + \left(\frac{4}{3}t\right)^{\frac{3}{2}}\right)^{\frac{1}{2}}\right\} \tag{7}$$

in particular, the tip of the corner, that we find in the direction of the corner bisector (given by $x = 0$) at each scale is provided by

$$\bar{x}(t) = \left(0, \lambda\left(\frac{4}{3}t\right)^{\frac{3}{4}}\right)$$

Since AMSS is Euclidean invariant, if the corner is centered in the point $\bar{x}_0$ and the corner bisector orientation is given by the unit vector $\hat{u}$ then, the corner evolution is given by Eq. (3).

3 Corner Estimation Algorithm Using AMSS

The proposed method for corner estimation can be divided in the following steps:

Step 1: Computation of the AMSS Scale Space. From the original image $u_0(\bar{x})$ we compute the AMSS scale space $u(t, \bar{x})$ using an explicit finite difference scheme.

Step 2: Initial Estimation of Potential Corners. We fix $t_0 \geq 0$ and we estimate an initial collection of potential corner tips $\{\bar{x}^k(t_0)\}_{k=1,\ldots,N_{t_0}}$ in the image as the local extrema (in the space variables) of the operator $(\mathcal{L}(u))^{\frac{1}{3}}(t_0, \bar{x})$. We observe that the computation of this operator is required in the AMSS estimation. Since we look for local extrema, the power $\frac{1}{3}$ is not relevant in this step. t_0 is a parameter of the algorithm and it is used to slightly smooth the image before corner estimation to avoid the computation of a lot of spurious

local extrema. We point out that, in contrast to other scale spaces, using AMSS we can recover the exact position of the corners in the original image from the position of the corners in the scale $t_0 > 0$. Indeed, using Eq. (3) we obtain that

$$\bar{x}_0 = \bar{x}(t_0) - \lambda \left(\frac{4}{3} t_0\right)^{\frac{3}{4}} \hat{u}, \tag{8}$$

Step 3: Tracking of Corners Across the AMSS Scale Space. Once the original collection of potential corners $\{\bar{x}^k(t_0)\}_{k=1,\dots,N_{t_0}}$ is estimated, we track the evolution of the corners across AMSS in the interval $[t_0, t^*]$ in the following iterative way: the interval $[t_0, t^*]$ is discretized using $\{t_n = t_0 + n \cdot \delta t\}_{n=0,\dots,N^*}$, where δt is the time step used to compute AMSS. Then, for any $n > 0$ the position of each corner tip $\bar{x}^k(t_n)$ at the scale t_n is obtained as the extremum of the operator $(\mathcal{L}(u))^{\frac{1}{3}}(t_n, \bar{x})$ in a neighborhood of $\bar{x}^k(t_{n-1})$ following the direction of $\nabla u(t_{n-1}, \bar{x}^k(t_{n-1}))$. During this tracking procedure spurious corner sequences are removed. For instance if $(\mathcal{L}(u))^{\frac{1}{3}}(t_n, \bar{x}^k(t_n))$ changes sign or becomes too small then the corner sequence is removed.

Step 4: Linear Approximation of AMSS Corner Evolution. For each corner sequence $\{\bar{x}^k(t_n)\}_{n=0,\dots,N^*}$, we compute a linear model (a_k, b_k) by minimizing the usual least squares approximation given by the error function

$$E(a,b) = \frac{\sum_{n=0}^{N^*} \left(\|\bar{x}^k(t_n) - \bar{x}^k(t_0)\| - (a(t_n{}^{\frac{3}{4}} - t_0{}^{\frac{3}{4}}) + b) \right)^2}{N^* + 1}, \tag{9}$$

that is, $(a_k, b_k) = \arg\min_{a,b} E(a,b)$. We observe that from the slope a_k and using the Eqs. (3) and (4) we can obtain λ_k and the corner angle. On the other hand we can compute the corner bisector unit vector $\hat{u}_k$ as a parallel vector to $x^k(t^*) - \bar{x}^k(t_0)$.

Step 5: Morphological Cornerness Measure and Corner Estimation. We point out that we can use the residual error $E(a_k, b_k)$ as a morphological cornerness measure. The lower the value of $E(a_k, b_k)$, the better the corner sequence fits the expected corner evolution. This cornerness measure is morphological in the sense that it is independent of the image grey value. It only depends on the shape of the corner evolution across AMSS. Therefore we can estimate the image corners by thresholding the residual error $E(a_k, b_k)$. In practice, we use a percentile of the values of $E(a_k, b_k)$ to estimate corners.

To represent a corner in an image we need the corner boundary lines. We observe that in our approach, for each corner, we always compute the slope parameter λ instead of the corner angle α. In the next straightforward lemma we show how to compute the corner boundary lines directly from λ.

Lemma 1. *Let $\hat{u}$ be a corner bisector and λ the slope parameter satisfying Eq. (4). Then, the vectors*

$$\hat{u}_-(\lambda) = \hat{u} - \frac{1}{\lambda^2}\hat{u}^\perp, \qquad \hat{u}_+(\lambda) = \hat{u} + \frac{1}{\lambda^2}\hat{u}^\perp,$$

are parallel to the corner boundary lines, that is, the angle between $\hat{u}$ and $\hat{u}_\pm(\lambda)$ is $\frac{\alpha}{2}$.

4 Experimental Setup

To check the accuracy of the proposed technique for a range of corners with different angles we use the collection of synthetic images of corners shown in Fig. 1. The corner angles range from 15 to 160°. In Fig. 2 we illustrate the result of the proposed technique for corner estimation for the 15° angle synthetic image. We present a zoom of the original image, the AMSS evolution for $t = 1$, the AMSS evolution for $t = 20$ and an illustration of the result of the proposed technique where we show the evolution of the corner location across AMSS for the scale interval [1,20] and the obtained corner angle obtained from the linear estimation (9). In Fig. 3 we illustrate for the 90° image the value of the operator $\mathcal{L}(u)^{\frac{1}{3}}(t, \bar{x})$ that we use as local cornerness measure to estimate and track the corner sequences.

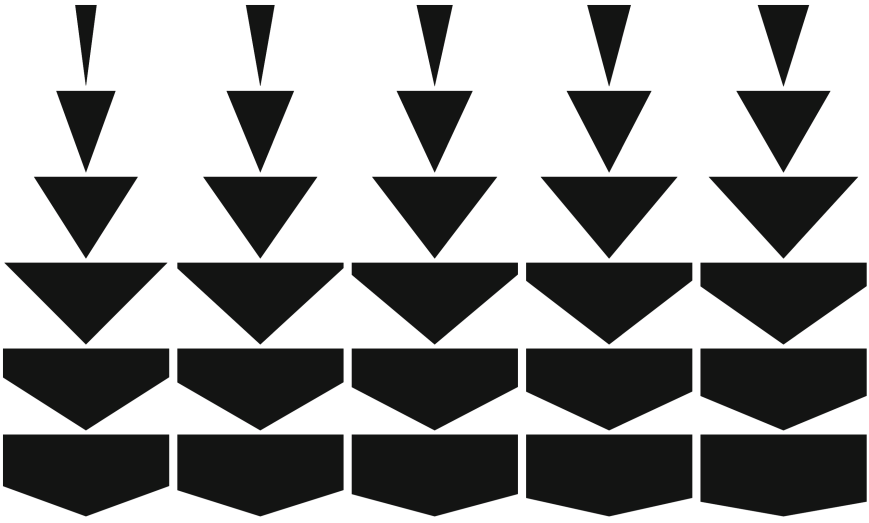

Fig. 1. Synthetic images of corners used in the experiments. The corner angles range from 15 to 160°.

In Fig. 4 we show, for the different synthetic angle images, the evolution of $\|\bar{x}(t) - \bar{x}_0\|$ with respect to $t^{\frac{3}{4}}$ for $t \in [0, 20]$. As expected by the result presented in Eq. (3), this evolution has a linear profile where the slope depends on the corner angle (the smaller the angle, the larger the slope). We observe that for small

Fig. 2. From left to right, we present a zoom of the 15° angle synthetic image, the AMSS evolution for $t = 1$, the AMSS evolution for $t = 20$ and an illustration of the result of the proposed technique where whe show the evolution of the corner location across AMSS for the scale interval [1,20] and the obtained corner angle obtained from the linear estimation (9).

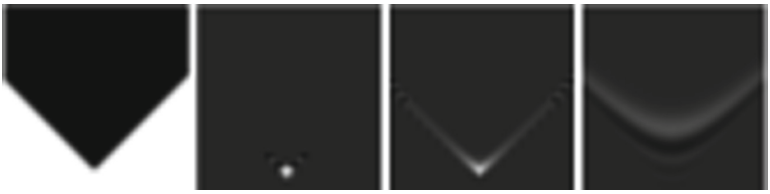

Fig. 3. From left to right we present a zoom of the 90° angle image and the result of the computation of the operator $\mathcal{L}(u)^{\frac{1}{3}}(t, \bar{x})$ for $t = 0, 1, 20$.

angles, the evolution shows a linear profile after a number of iterations of AMSS. This is due to the fact that corner angles are represented as discrete synthetic images which introduce discretization errors (specially for small angles), so in this case a number of AMSS iterations are required to regularize the image corner contours. Therefore we use the AMSS evolution in $[0, t_0]$ as a regularization step. This approach presents also the advantage that we can detect multiple junctions. Indeed, using AMSS, a multiple junction is managed as a collection of corners sharing the same corner tip. As the evolution of the corners in a multiple junction moves in different directions, after a time t_0 the location of the corners will be different and then the method can detect each corner independently as different local extrema of the operator $(\mathcal{L}(u))^{\frac{1}{3}}(t_0, \bar{x})$.

In Fig. 5 we illustrate the evolution across AMSS of the value of the differential operator $(\mathcal{L}(u))^{\frac{1}{3}}$ in the corner tip for the different angles. We observe, due to the regularization effect of AMSS, an exponential decay of the evolution profile.

In Fig. 6 we illustrate the quality of the above linear approximation. We show, for the different angles, the average residual error $E(a, b)$ defined in (9) obtained using the linear approximation of $\|\bar{x}(t) - \bar{x}(t_0)\|$ with respect to $t^{\frac{3}{4}} - t_0^{\frac{3}{4}}$ for $t \in [1, 20]$. As expected (looking at the results of Fig. 4) we observe that the average residual error $E(a, b)$ is quite small (below 0.01) and the results are worse for very small or large angles where the numerical discretization to generate the synthetic image angles introduces more errors.

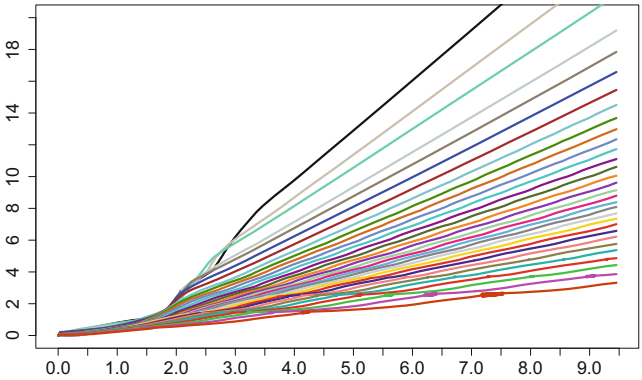

Fig. 4. For the corner images in Fig. 1 we plot the evolution of $\|\bar{x}(t) - \bar{x}_0\|$ with respect to $t^{\frac{3}{4}}$ for $t \in [0, 20]$.

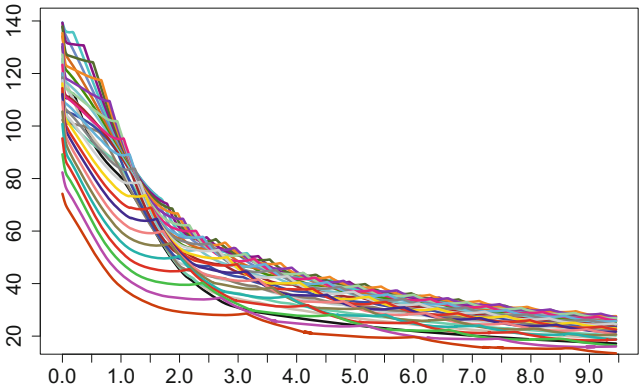

Fig. 5. For the corner images in Fig. 1 we plot the evolution of the differential operator $\mathcal{L}(u)^{\frac{1}{3}}(\bar{x}(t))$ with respect to $t^{\frac{3}{4}}$ for $t \in [0, 20]$.

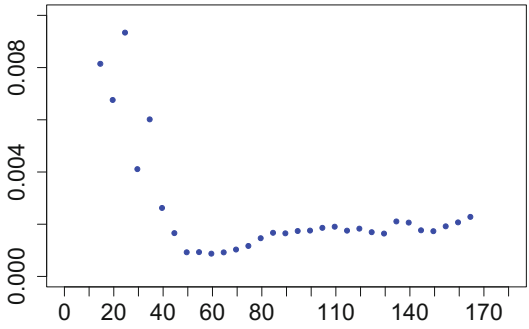

Fig. 6. For the corner images in Fig. 1 we plot, with respect to the angle (in degrees), the average residual error $E(a, b)$ defined in (9) obtained using the linear approximation of $\|\bar{x}(t) - \bar{x}(t_0)\|$ with respect to $t^{\frac{3}{4}} - t_0{}^{\frac{3}{4}}$ for $t \in [1, 20]$.

Using Eqs. (3) and (4) we can compute, for each synthetic image angle, from the slope of the linear approximation of $\|\bar{x}(t) - \bar{x}(t_0)\|$ with respect to $t^{\frac{3}{4}} - t_0{}^{\frac{3}{4}}$, the corner angle α or equivalently the parameter λ. In Fig. 7 we compare, for the range of angles, the parameter λ obtained using the slope of the linear approximation and the actual value obtained from the angle using Eq. (4). Due to discretization errors, we can observe a systematic bias between the estimation and the actual value of λ. However, this bias can be properly corrected using a basic linear regression approximation. With a "R-squared" value of 0.9998931 we obtain the following linear model to correct the systematic error in the estimation of λ from the one obtained using the estimated slope

$$\lambda = 0.071917 + 1.029484\bar{\lambda} \tag{10}$$

where $\bar{\lambda}$ represents the original estimation using the estimated slope and λ the corrected one. In Fig. 7 we also illustrate the correction in the estimation of λ using the above linear model.

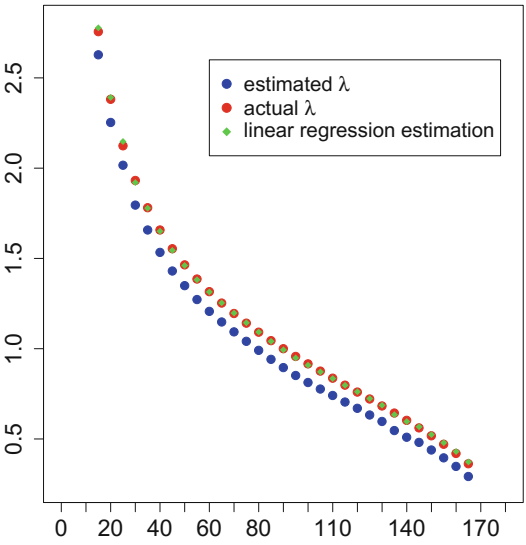

Fig. 7. For the corner images in Fig. 1 we plot, with respect to the angle (in degrees), the initial estimation of the λ corner parameter using a linear approximation of the evolution of $\|\bar{x}(t) - \bar{x}(t_0)\|$ with respect to $t^{\frac{3}{4}} - t_0^{\frac{3}{4}}$ for $t \in [t_0, 20]$ with $t_0 = 1$. The actual value of λ according to the corner angle (computed using Eq. (4)) and the correction of the initial estimation using a linear regression approach.

In Fig. 8 we show for the different angles, the error (in pixels) of the corner location estimation $\bar{x}_0$ using the proposed method for the scale interval [1,20] and the error obtained using the standard Harris method with $\sigma = 1$ (the standard deviation of the Gaussian convolution kernel used to compute the structure

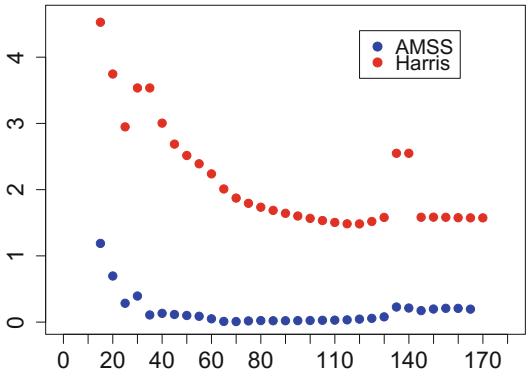

Fig. 8. For the corner images in Fig. 1 we plot, with respect to the angle (in degrees), the error (in pixels) of the corner location estimation $\bar{x}_0$ using AMSS with the scale interval $t \in [1, 20]$ and the standard Harris method.

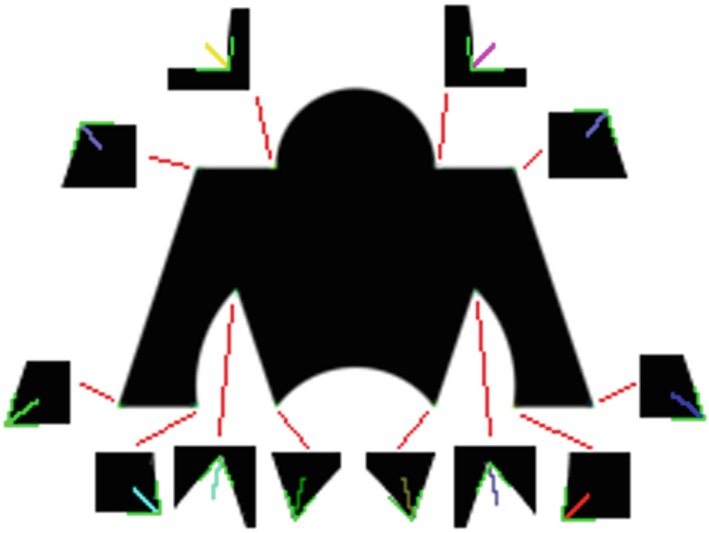

Fig. 9. We illustrate the results of the proposed method for a synthetic image including different types of corner structures using as scale interval [1,20]. We present a zoom of the corner areas where the evolution of the corner tips across AMSS and the obtained corner boundary lines are illustrated.

tensor). To estimate accurately the corner tip location in the original image from its estimation in $t_0 = 1$ we use Eq. (8). We point out that the corner estimation using AMSS is much more accurate than the one obtained by the Harris method. The main reason is that the Gaussian convolution required in Harris method moves the corners introducing errors in the corner locations. Moreover these

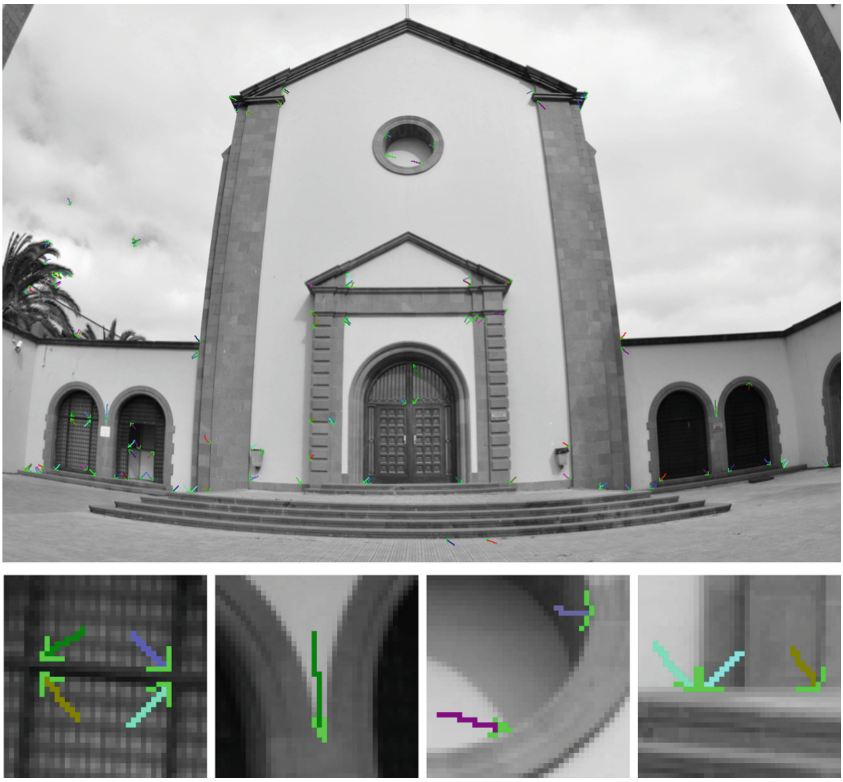

Fig. 10. We illustrate the results of the proposed method for a real image using as scale interval [1,20]. We also present a zoom of some corner areas.

errors can not be corrected as in the case of AMSS because there are not explicit formula to measure the corner location displacement produced by the Harris method. We observe that in both methods the errors are larger in the case of small angles where the discrete representation of the angle as an image includes large discretization errors.

In Fig. 9 we illustrate the results of the proposed method for a synthetic image including different types of corner structures.

In Fig. 10 we present an application of the proposed technique to a real image where we use a percentile of the residual average error $E(a, b)$ given by (9) to choose the most relevant corners in the image. As illustrated in the figure, the method is able to handle multiple junctions automatically without any further analysis.

5 Conclusions

In this paper we introduce a morphological cornerness measure based on the expected evolution of an ideal corner across AMSS. The main advantange of AMSS is that in this scale space we have closed-form expressions for the corner evolution and this is something unique to AMSS which allow us to develop accurate corner location estimation techniques. Moreover, using AMSS we can handle automatically more complex structures as multiple junctions. We propose a new method to track corners across AMSS based on the local extrema of the operator $\mathcal{L}(u)$ defined in (2). We present a detailed experimental study of the accuracy of the proposed method using a collection of synthetic corners using different angles. We show that the proposed method is much more accurate than the usual Harris technique. To attain such level of accuracy we use that in AMSS we can go backwards in the scale to recover the original corner location from its location at any scale (something unique to AMSS). We also present experiments in real images which show that the proposed method strongly simplifies the number of corners providing the most significant ones.

Acknowledgement. This research has partially been supported by the MINECO project reference MTM2016-75339-P (AEI/FEDER, UE) (Ministerio de Economía y Competitividad, Spain).

References

1. Alvarez, L., Cuenca, C., Esclarín, J., Mazorra, L., Morel, J.M.: Affine invariant distance using multiscale analysis. J. Math. Imaging Vis. **55**(2), 199–209 (2016)
2. Alvarez, L., Guichard, F., Lions, P.L., Morel, J.M.: Axiomatisation et nouveaux opérateurs de la morphologie mathématique. Comptes rendus de l'Académie des sciences. Série 1, Mathématique **315**(3), 265–268 (1992)
3. Alvarez, L., Guichard, F., Lions, P.L., Morel, J.M.: Axiomes et équations fondamentales du traitement d'images. (analyse multiéchelle et edp). Comptes rendus de l'Académie des sciences. Série 1, Mathématique **315**(2), 135–138 (1992)
4. Alvarez, L., Guichard, F., Lions, P.L., Morel, J.M.: Axioms and fundamental equations of image processing. Arch. Ration. Mech. Anal. **123**(3), 199–257 (1993)
5. Alvarez, L., Morales, F.: Affine morphological multiscale analysis of corners and multiple junctions. Int. J. Comput. Vis. **25**(2), 95–107 (1997)
6. Angenent, S., Sapiro, G., Tannenbaum, A.: On the affine heat equation for non-convex curves. J. Am. Math. Soc. **11**(3), 601–634 (1998)
7. Demetz, O., Hafner, D., Weickert, J.: Morphologically invariant matching of structures with the complete rank transform. Int. J. Comput. Vis. **113**(3), 220–232 (2015)
8. Harris, C., Stephens, M.: A combined corner and edge detector. In: Proceedings of Fourth Alvey Vision Conference, pp. 147–151 (1988)
9. Lowe, D.G.: Distinctive image features from scale-invariant keypoints. Int. J. Comput. Vis. **60**(2), 91–110 (2004)
10. Mokhtarian, F., Suomela, R.: Robust image corner detection through curvature scale space. IEEE Trans. Pattern Anal. Mach. Intell. **20**(12), 1376–1381 (1998)

11. Osher, S., Sethian, J.A.: Fronts propagating with curvature-dependent speed: algorithms based on Hamilton-Jacobi formulations. J. Comput. Phys. **79**(1), 12–49 (1988)
12. Sapiro, G., Tannenbaum, A.: On affine plane curve evolution. J. Funct. Anal. **119**(1), 79–120 (1994)
13. Sapiro, G., Tannenbaum, A.: Affine invariant scale-space. Int. J. Comput. Vis. **11**(1), 25–44 (1993)
14. Yu, G., Morel, J.M.: ASIFT: an algorithm for fully affine invariant comparison. Image Proces. On Line **1**, 11–38 (2011)